7-27-2018

Effective Demagnetizing Factors of Diamagnetic Samples of Various Shapes

Ruslan Prozorov
Iowa State University and Ames Laboratory, prozorov@ameslab.gov

Vladimir G. Kogan
Ames Laboratory, kogan@ameslab.gov

Effective Demagnetizing Factors of Diamagnetic Samples of Various Shapes

Abstract
Effective demagnetizing factors that connect the sample magnetic moment with the applied magnetic field are calculated numerically for perfectly diamagnetic samples of various nonellipsoidal shapes. The procedure is based on calculating the total magnetic moment by integrating the magnetic induction obtained from a full three-dimensional (3D) solution of the Maxwell equations using an adaptive mesh. The results are relevant for superconductors (and conductors in ac fields) when the London penetration depth (or the skin depth) is much smaller than the sample size. Simple but reasonably accurate approximate formulas are given for practical shapes including rectangular cuboids, finite cylinders in axial and transverse fields, as well as infinite rectangular and elliptical cross-section strips.

Disciplines
Condensed Matter Physics | Metallurgy | Physics

Effective Demagnetizing Factors of Diamagnetic Samples of Various Shapes

R. Prozorov[1,2,*] and V. G. Kogan[1]

[1]*Ames Laboratory, Ames, Iowa 50011, USA*

[2]*Department of Physics & Astronomy, Iowa State University, Ames, Iowa 50011, USA*

(Received 16 December 2017; revised manuscript received 18 March 2018; published 27 July 2018)

Effective demagnetizing factors that connect the sample magnetic moment with the applied magnetic field are calculated numerically for perfectly diamagnetic samples of various nonellipsoidal shapes. The procedure is based on calculating the total magnetic moment by integrating the magnetic induction obtained from a full three-dimensional (3D) solution of the Maxwell equations using an adaptive mesh. The results are relevant for superconductors (and conductors in ac fields) when the London penetration depth (or the skin depth) is much smaller than the sample size. Simple but reasonably accurate approximate formulas are given for practical shapes including rectangular cuboids, finite cylinders in axial and transverse fields, as well as infinite rectangular and elliptical cross-section strips.

DOI: 10.1103/PhysRevApplied.10.014030

I. INTRODUCTION

The correction of results of magnetic measurements for the distortion of the magnetic field inside and around a finite sample of arbitrary shape is not trivial, but is a necessary part of experimental studies in magnetism and superconductivity. The internal magnetic field is uniform only in ellipsoids (see Fig. 2), for which demagnetizing factors can be calculated analytically [1,2]. In general, however, the magnetic field is highly nonuniform inside and outside of finite samples of arbitrary (nonellipsoidal) shape and various approaches have been used to handle the problem [3–9]. As discussed below, the major obstacle has been that, so far, it has not been possible to calculate the total magnetic moment of arbitrary-shaped samples and approximations and assumptions have had to be made. As a result, various approximate demagnetizing factors have been introduced. For example, the so-called "magnetometric" demagnetizing factor, N_m, is based on equating the magnetostatic self-energy to the energy of a fully magnetized ferromagnetic prism or, more generally, considering volume-average magnetization in magnetized [4,5,7] or perfectly diamagnetic [6] media. Similarly, the so-called "fluxmetric" or "ballistic" demagnetizing factor, N_f, is based on the average magnetization in the sample midplane [4,6]. In these formulations, micromagnetic calculations are used to find the distribution of the surface magnetic dipole density that satisfies the boundary conditions and the assumptions made. Then the average magnetization is calculated and used to compute the N factors, using formulas similar to those used in this work. One common, but generally incorrect, assumption is that the sum of the demagnetizing factors along the three principal axes equals one. This is true only for ellipsoids. Notably, Brandt [9] has used a different approach by numerically calculating the slope, dm/dH_0, of the magnetic moment m vs the applied magnetic field H_0 in a perfect superconductor in the Meissner state to compute the approximate N factors for a two-dimensional (2D) situation of infinitely long strips of rectangular cross section in the perpendicular field and he extended these results to finite 3D cylinders (also of rectangular cross section) in the axial magnetic field. We find excellent agreement between our calculations and Brandt's results for these geometries. Also, in our earlier work, the 2D numerical solutions of the Maxwell equations obtained using the finite element method were generalized to 3D cylinders and yielded similar results [10]).

Yet, despite multiple attempts, the results published so far do not describe three-dimensional finite samples of arbitrary nonellipsoidal shapes to answer an important practical question: What is the *total magnetic moment* of a three-dimensional sample of a particular shape in a fixed *applied* magnetic field, $\boldsymbol{H}_0$? We answer this question by finding a way to calculate the total magnetic moment from first principles with no assumptions and introducing the *effective* demagnetizing factors without referring to the details of the spatial distribution of the magnetic induction. We will first consider how these effective demagnetizing factors depend on the finite magnetic permeability, μ_r, which highlights the difference between ellipsoidal and nonellipsoidal shapes. Complete treatment of finite μ_r will require separate papers, in which we will focus on (a) the London-Meissner state in superconductors of arbitrary shape with a finite London penetration depth and

*Corresponding author. prozorov@ameslab.gov

(b) demagnetizing corrections in local and linear magnetic media with arbitrary μ_r.

In this work, we focus on perfectly diamagnetic samples, inside which the magnetic induction $B = 0$, which allows the study of pure effects of the sample shape. The results can be used for the interpretation of magnetic measurements of superconductors when the London penetration depth is much smaller than the sample dimensions (usually, a good approximation almost up to $0.95T_c$) or in conducting samples subject to an ac magnetic field when the skin depth is small. Our goal is to find simple-to-use, but sufficiently accurate, approximate formulas suitable for the calculation of the demagnetizing correction for many shapes that can approximate realistic samples, such as finite cylinders and cuboids (rectangular prisms).

II. DEFINITIONS

In local and magnetically linear media without demagnetizing effects (an infinite slab or cylinder in a parallel magnetic field),

$$B = \mu H = \mu_0(M + H), \tag{1}$$

$$M = \frac{B}{\mu_0} - H = \chi H, \tag{2}$$

where $\mu_0 = 4\pi \times 10^{-7}$ (N/A^2 or H/m) is the magnetic permeability of free space; μ and χ are the linear magnetic permeability and susceptibility (in general, these quantities are second-rank tensors, but here we consider the isotropic case).

It follows, then, that

$$\chi = \frac{\mu}{\mu_0} - 1 = \mu_r - 1, \tag{3}$$

where $\mu_r = \mu/\mu_0$ is the relative magnetic permeability; $\mu_r = 1$ for nonmagnetic media and $\mu_r = 0$ and $\chi = -1$ for a perfect diamagnet.

For finite samples of ellipsoidal shape, *constant* demagnetizing factors N connect the applied magnetic field H_0 along a certain principal direction with the internal field, H,

$$H = H_0 - N, M, \tag{4}$$

and in terms of an applied field the magnetization is as follows:

$$M = \frac{\chi}{1 + \chi N} H_0. \tag{5}$$

In arbitrary-shaped samples, this simple description breaks down and we have to introduce similarly structured effective equations, albeit *applicable only for integral quantities*. Namely, upon application of an external field H_0, a finite sample of a given shape develops a measurable total magnetic moment m. We now *define* the "effective" (or "integral," or "apparent") magnetic susceptibility, χ_0, and the corresponding demagnetizing factor, N, by writing relations that are structurally similar to Eq. (5):

$$m = \chi_0 H_0 V = \frac{\chi H_0 V}{1 + \chi N}, \tag{6}$$

which reduces to conventional equations in the case of a linear magnetic material of ellipsoidal shape. Importantly, Eq. (6) contains only one property to be determined—the intrinsic susceptibility, χ—provided that the demagnetizing factor N can be calculated for a given geometry. This can be done for model materials with known (assumed) χ and numerically evaluated χ_0 by inverting Eq. (6) to obtain

$$N = \frac{1}{\chi_0} - \frac{1}{\chi}, \tag{7}$$

where $-1 \le \chi \le \infty$ and $-\infty \le \chi_0 \le \chi$. To eliminate the influence of the material, for calculations of N we will consider a perfect diamagnet with $\chi = -1$, so that when $\chi_0 = \chi = -1, N = 0$, as it should in the case of no demagnetizing effects (an infinite slab or a cylinder in a parallel field), and $N \to 1$ for an infinite plate in a perpendicular field where $\chi_0 \to -\infty$, while χ still equals -1.

The main issue in using Eq. (7) to calculate demagnetizing factors is to calculate the total magnetic moment of a sample of a given (arbitrary) shape. There are two ways of approaching this. In nonmagnetic (super)conductors, one first solves Maxwell equations with the help of one of the existing numerical software packages (such as COMSOL [11]), to find the current density $\boldsymbol{j}(\boldsymbol{r})$. Then, the total magnetic moment is given by [1]

$$\boldsymbol{m} = \frac{1}{2}\int [\boldsymbol{r} \times \boldsymbol{j}(\boldsymbol{r})] dV. \tag{8}$$

The integral here can be evaluated over the entire space, but the integrand is nonzero only inside the sample where the currents flow.

The second way to calculate the total magnetic moment, $\boldsymbol{m}$, is given by

$$\boldsymbol{m} = \alpha \int \left[\frac{\boldsymbol{B}(\boldsymbol{r})}{\mu_0} - \boldsymbol{H}_0\right] d^3\boldsymbol{r}, \tag{9}$$

where $\boldsymbol{B}(\boldsymbol{r})$ is the actual field (magnetic induction) and $\boldsymbol{H}_0$ is the uniform applied magnetic field. Here, the integral must be evaluated in a region that includes the sample (this can be the entire space). We show in the next section that this integral is not unique, but depends on the method chosen for the integration. This is accounted for by a constant α in Eq. (9), $\alpha = 3/2$ for integration over the large spherical domain that includes the whole sample, whereas $\alpha = 1$ for the integration domain as a large cylinder with

its axis parallel to $\boldsymbol{H}_0$. It turns out that for numerical reasons, the cylindrical domain is preferable and we use it for our numerical work. Equation (9) is central to the present work, because it allows calculations without use of the current distribution. This equation (with $\alpha = 3/2$) can be found as Eq. (5.62) in Jackson [12]. A related discussion about the multipole representation of the field outside the region where the field sources are localized is given in Ref. [13].

For evaluation of $\boldsymbol{B}(\boldsymbol{r})$, one can use an approximation of a fully diamagnetic sample imposing "magnetic shielding" boundary conditions, which is available in the COMSOL software. Employing Eq. (9) with $\boldsymbol{B}(\boldsymbol{r})$ simplifies the numerical procedure and improves the accuracy considerably. However, the proof of Eq. (9) is not at all trivial and we derive it analytically in the next section. We also verify the results by calculating the total magnetic moment $\boldsymbol{m}$ utilizing both approaches: evaluating the current distribution in superconducting samples using the London equations and employing Eq. (8), and using a COMSOL-generated field distribution $\boldsymbol{B}(\boldsymbol{r})$ and Eq. (9).

III. THE TOTAL MAGNETIC MOMENT $\boldsymbol{m}$

According to Jackson [12], the magnetic moment $\boldsymbol{m}$ of the current distribution induced by an applied uniform field $\boldsymbol{H}_0$ in a finite sample is related to the distribution of the magnetic induction $\boldsymbol{B}(\boldsymbol{r})$ by

$$\boldsymbol{I} = \int_{\mathcal{R}} \left[\frac{\boldsymbol{B}(\boldsymbol{r})}{\mu_0} - \boldsymbol{H}_0 \right] d^3\boldsymbol{r} = \frac{2}{3}\,\boldsymbol{m}. \tag{10}$$

where $\mathcal{R}$ is a radius of a large sphere containing the whole sample. In particular, $\mathcal{R}$ can be infinite, e.g., the integral can be extended to the whole space. This relation is central for our calculations, so that we can provide a more general derivation than that given in Ref. [12]. We show that, depending on the method chosen to evaluate the integral $\boldsymbol{I}$ over the whole space, Eq. (9) can have different forms, parameterized by a factor α.

The field $\boldsymbol{B}$ consists of the applied field $\boldsymbol{H}_0$ and the field $\boldsymbol{h}$ due to currents $\boldsymbol{j}$ in the sample of a finite volume V:

$$\frac{\boldsymbol{B}}{\mu_0} = \boldsymbol{H}_0 + \boldsymbol{h}, \tag{11}$$

i.e., $\boldsymbol{I} = \int \boldsymbol{h}\, d^3\boldsymbol{r}$, where, according to the Biot-Savart law,

$$\boldsymbol{h}(\boldsymbol{r}) = \frac{1}{4\pi} \int_V d^3\boldsymbol{\rho} \frac{\boldsymbol{j}(\boldsymbol{\rho}) \times \boldsymbol{R}}{R^3}, \quad \boldsymbol{R} = \boldsymbol{r} - \boldsymbol{\rho}. \tag{12}$$

Hence, we have

$$\begin{aligned} 4\pi \boldsymbol{I} &= \int_{\mathcal{R}} d^3\boldsymbol{r} \int_V d^3\boldsymbol{\rho} \frac{\boldsymbol{j}(\boldsymbol{\rho}) \times \boldsymbol{R}}{R^3} \\ &= \int_V d^3\boldsymbol{\rho}\, \boldsymbol{j}(\boldsymbol{\rho}) \times \int_{\mathcal{R}} d^3\boldsymbol{r} \frac{\boldsymbol{R}}{R^3} \\ &= \int_V d^3\boldsymbol{\rho}\, \boldsymbol{j}(\boldsymbol{\rho}) \times \mathcal{E}(\boldsymbol{\rho}). \end{aligned} \tag{13}$$

where we introduce the "pseudoelectric field," $\mathcal{E}(\boldsymbol{\rho}) = \int d^3\boldsymbol{r}\boldsymbol{R}/R^3$, which is analogous to the electrostatic field of a uniform charge distribution with a constant density of -1 over the whole space. For $\boldsymbol{\rho} = 0$, we must have $\mathcal{E} = \int d^3\boldsymbol{r}(\boldsymbol{r}/r^3) = 0$ by symmetry. For such a distribution, the field $\mathcal{E}$ is not defined uniquely: it depends on the way one *divides* the space in the charged elements.

If one uses elements as spherical shells, and applies the Gauss theorem to a sphere of a radius $\boldsymbol{\rho}$, one obtains

$$\mathcal{E} = -\frac{4\pi}{3}\boldsymbol{\rho}. \tag{14}$$

Hence, we have

$$\boldsymbol{I} = -\frac{1}{3}\int_V d^3\boldsymbol{\rho}\, \boldsymbol{j}(\boldsymbol{\rho}) \times \boldsymbol{\rho} = \frac{2}{3}\boldsymbol{m}, \tag{15}$$

where $\boldsymbol{m}$ is the total magnetic moment. It is worth noting that this formula holds for any current distribution within a finite sample of arbitrary shape.

If one uses integration elements as cylindrical shells parallel to $\boldsymbol{H}_0$, i.e., one chooses the volume element as $2\pi\rho_1\, d\rho_1 dz$ (in which $\boldsymbol{\rho}_1$ is the cylindrical radius vector) and applies the Gauss theorem to a cylinder of a radius ρ, one obtains

$$\mathcal{E} = -2\pi\boldsymbol{\rho}_1. \tag{16}$$

Substituting this in Eq. (13), one expresses the z component of the integral $\boldsymbol{I}$:

$$I_z = m_z. \tag{17}$$

It is easy to show that the region where the integral $\boldsymbol{I}$ is evaluated can be taken as a sphere (or a cylinder) of a radius $\mathcal{R}_1$ that contains the entire sample of interest within this region. Then, if one takes a larger radius $\mathcal{R}_2$, the layer between spheres (cylinders) $\mathcal{R}_1$ and $\mathcal{R}_2$ does not contribute to the effective field $\mathcal{E}$ because the "electric field" of such a uniformly charged spherical (cylindrical) shell $\mathcal{E}(r) = 0$ for $r < \mathcal{R}_1$.

In Appendix A, for demonstration purposes, we evaluate the integral $\boldsymbol{I}$ both analytically and numerically for spherical and cylindrical integration volumes for the case of a current ring for which the distribution of $\boldsymbol{B}(\boldsymbol{r})$ is known.

It is worth mentioning that a similar argument can be applied for evaluation of the dipole moment of a metallic sample of arbitrary shape placed in a uniform electric field $\boldsymbol{E}_0$, $\boldsymbol{d} = \int d^3\boldsymbol{\rho}\, n(\boldsymbol{\rho})\boldsymbol{\rho}$ [in which $n(\boldsymbol{\rho})$ is the charge density, for point charges $\boldsymbol{d} = \sum_v e_v \boldsymbol{\rho}_v$]. It is straightforward to see that

$$\boldsymbol{d} \propto \int d^3\boldsymbol{\rho}[\boldsymbol{E}(\boldsymbol{\rho}) - \boldsymbol{E}_0]. \tag{18}$$

Here, $\boldsymbol{E}(\boldsymbol{\rho})$ is the electric-field distribution, which can be found numerically with the help of software similar to COMSOL [11]. As in the magnetic case, the integration here can be done over a spherical (or cylindrical) region that contains the whole sample. The coefficient of proportionality here is $2\alpha/\epsilon_0$, where α is given above and ϵ_0 is the vacuum dielectric constant. This result might be useful in problems such as those considered in Ref. [14].

In Appendix B, we provide a derivation of Eq. (9) in Gaussian units for readers who prefer CGS in general electromagnetic problems.

IV. NUMERICAL CALCULATIONS

Numerical calculations of the three-dimensional distribution of vector $\boldsymbol{B}(\boldsymbol{r})$ are performed with the COMSOL software [11] using an adaptive finite-element solution of the Maxwell equations in a form applicable to many different situations, including external currents $\boldsymbol{j}_{\text{ext}}$ and electrical conductivity σ in the case of conducting materials:

$$\begin{aligned} \nabla \times \boldsymbol{H} &= \boldsymbol{j}, \\ \boldsymbol{B} &= \nabla \times \boldsymbol{A}, \\ \boldsymbol{j} &= \sigma \boldsymbol{E} + \boldsymbol{j}_{\text{ext}}, \\ \boldsymbol{B} &= \mu_0 \mu_r \boldsymbol{H}, \end{aligned} \tag{19}$$

We use finite μ_r in the next section to illustrate the μ_r-dependent effective demagnetizing factor. Otherwise, throughout, $\mu_r = 0$, $\sigma = 0$ and $\boldsymbol{j}_{\text{ext}} = 0$. For details, the reader is referred to extensive documentation available on the COMSOL web site [11]. The COMSOL "ac/dc magnetic field" module is used, in a stationary dc study, to model perfect diamagnetic material. A frequency-dependent ac study is used to formulate the London equations, with a complex frequency-dependent conductivity. In the limit of a perfect diamagnetic material, both approaches give identical results.

The main numerical difficulty is to construct the proper adaptive mesh, which should be fine enough to resolve surface currents, but still give solutions in reasonable time. Various strategies can be employed to optimize the process, utilizing symmetries, periodic boundary conditions, perfect magnetic shielding, and various adaptive sweeps and batch modes. Each geometry is solved for by using several different approaches and different meshes to make sure that the final results are model independent. Geometries for which analytic solutions are known (ellipsoids and cylinders) are used to verify the numerical schemes and give nearly perfect agreement. All calculations are done in SI units, so that the factor μ_0 is properly taken into account where required.

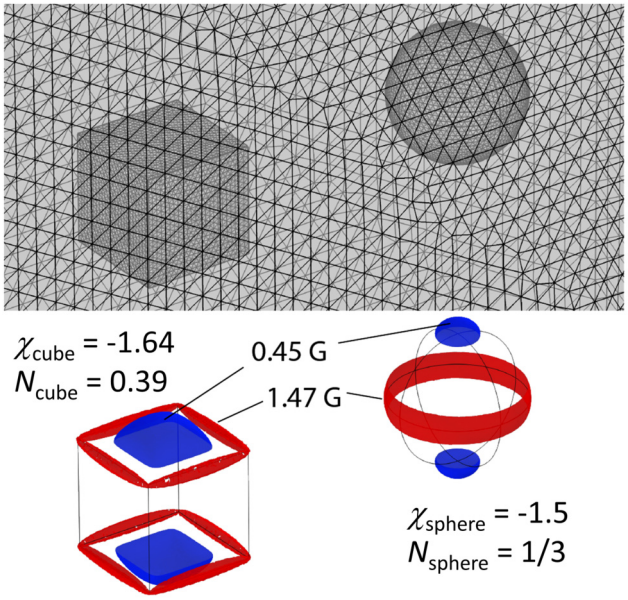

FIG. 1. Top panel: a sphere and a cube in a full three-dimensional meshed model. Bottom panel: the corresponding 3D solutions, showing surfaces of constant-amplitude magnetic induction of 0.45 G and 1.47 G. The applied external field is 1 Oe.

To illustrate the method, the top panel of Fig. 1 shows a three-dimensional meshed sphere (right) and cube (left). The meshes used in actual calculations are much finer and contain various adaptive refinements and layers (they would be irresolvably dark if shown here). The bottom panel of Fig. 1 shows two surfaces of constant magnetic induction around these samples. With the applied field of 1 Oe $\approx$ 79.58 A/m, one surface with 0.45 G = 0.045 mT corresponds to diamagnetic shielding outside the sample, while 1.47 G = 0.147 mT corresponds to enhancement due to demagnetization. Clearly, the cube provides more shielding, $\chi_0 = \chi_{\text{cube}} = -1.64$, compared to the sphere, $\chi_0 = \chi_{\text{sphere}} = -1.5$, and this is reflected in a larger demagnetizing factor, $N_{\text{cube}} = 0.39$ compared to $N_{\text{sphere}} = 1/3$. It is already obvious here that for a cube, due to symmetry, the sum of the demagnetizing factors in the three principal directions is $\sum N_i = 3 \times 0.39 = 1.17 > 1$.

V. THE FINITE MAGNETIC PERMEABILITY

Unfortunately, complications arise in nonellipsoidal samples with finite magnetic permeability. While demagnetizing

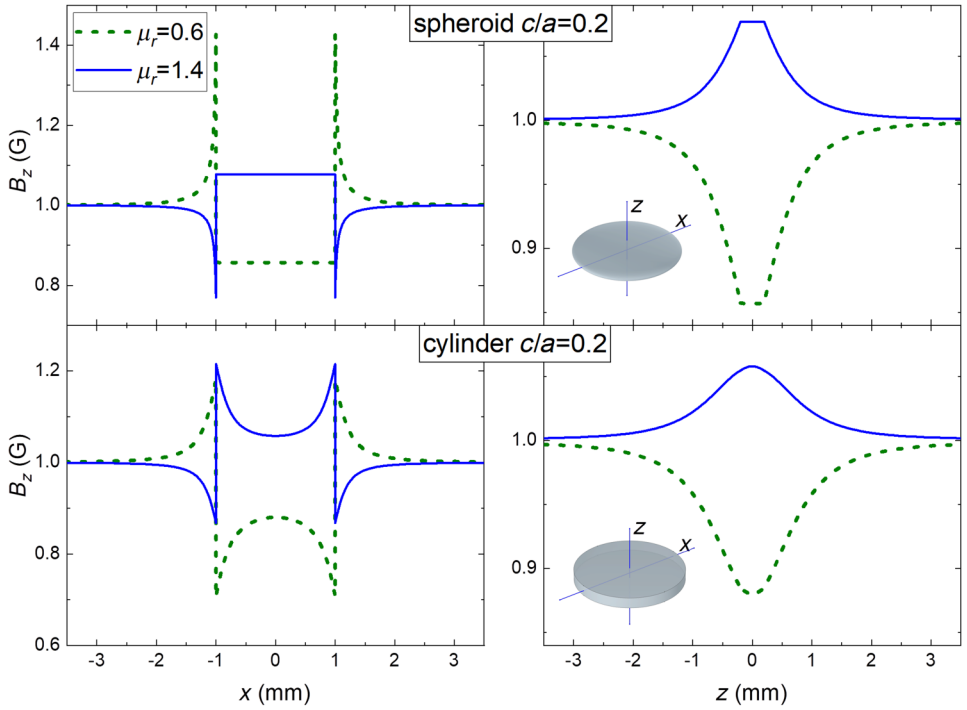

FIG. 2. The B_z component of the magnetic induction across the sample in the x direction (left-hand panels) and in the z direction (right-hand panels) for two values of the relative magnetic permeability, $\mu_r = 0.6$ (diamagnetic, dashed lines) and $\mu_r = 1.4$ (paramagnetic, solid lines). The top panels are for an oblate spheroid and the bottom panels are for a cylinder of the same aspect ratio (see the insets). Note the constant field inside a spheroid and the strongly nonuniform magnetic induction inside a cylinder.

factors are constants independent of μ_r in ellipsoidal samples, they become μ_r-dependent otherwise. Hence, effective demagnetizing factors are no longer purely geometric parameters. It is still possible to provide some practical approximation of this behavior, but this will require a separate paper.

Here, we outline all the steps of calculating effective demagnetizing factors. First, we use COMSOL to calculate the three-dimensional distribution of the vector $\boldsymbol{B}(\boldsymbol{r})$ inside and outside the sample. We do this for two values of the magnetic permeability corresponding to diamagnetic and paramagnetic materials. Figure 2 shows the B_z component of the magnetic induction across the sample in the x direction, $B_z(x, z = 0)$ (left-hand panels), and in the z direction, $B_z(x = 0, z)$ (right-hand panels), for two values of the relative magnetic permeability, $\mu_r = 0.6$ (diamagnetic, dashed lines) and $\mu_r = 1.4$ (paramagnetic, solid lines). The top panels are for an oblate spheroid and the bottom panels are for a very nonuniform induction inside a cylinder.

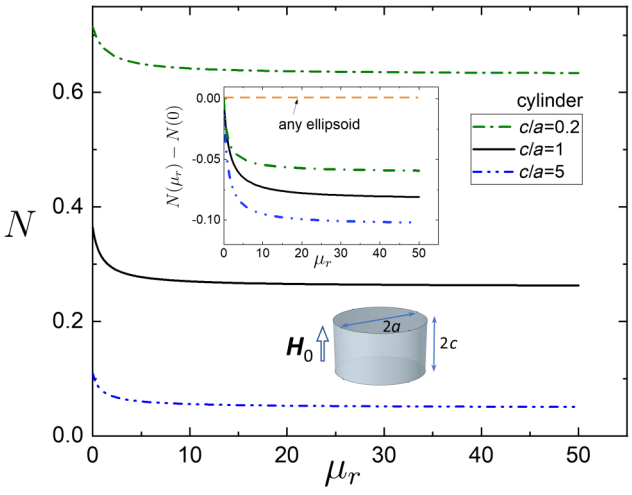

FIG. 3. The effective demagnetizing factor N for a finite cylinder in an axial magnetic field for three different aspect ratios as a function of the relative magnetic permeability μ_r. The inset shows the difference $N(\mu_r) - N(0)$.

The next step is to use Eq. (9) with spherical or cylindrical integration volumes to compute the total magnetic moment in a fixed applied field of 1 Oe. Finally, we use Eq. (7) to evaluate the effective demagnetizing factor.

Figure 3 shows the μ_r dependence of the effective demagnetizing factor $N(\mu_r)$ of a finite cylinder in a longitudinal magnetic field for three different values of the thickness-to-radius aspect ratio. The inset shows the variation of the difference $N(\mu_r) - N(0)$. As expected [see Eq. (7)], for a strongly paramagnetic material with $\mu_r > 5 - 10$, the variation in N is not too substantial. However, for materials of practical interest, where $0 \leq \mu_r \leq 10$, the dependence of N on μ_r is quite strong. We will attempt to provide a simplified description of $N(\mu_r)$ for various nonellipsoidal shapes elsewhere.

VI. PERFECT DIAMAGNETS

For now, we will focus on a perfect diamagnetic material with constant $B = 0$ inside.

A. The general ellipsoid

Throughout this paper, we adopt a uniform designation of sample dimensions $2a \times 2b \times 2c$ along the Cartesian x, y, and z axes, with an external magnetic field applied along the z axis, parallel to the side c of the sample. Also, we will always use the dimensionless ratios b/a and c/a.

For completeness, it is useful to show here the analytic solution for the ellipsoid with semiaxes, a, b, and c given in Eqs. (4.5) and (4.25) of Ref. [1]. Osborn [2] also gives analytic solutions of this case, expressed via the differences of incomplete elliptic integrals and written for a restricting case of $a \geq b \geq c$ in his Eqs. (2.1)–(2.6). It turns out that the formulas given in Landau's book are much easier to compute numerically and they work for any ratio of the dimensions [1]. The demagnetizing factor along the c axis is as follows:

$$N_{\text{ellipsoid}} = \frac{1}{2}\frac{b}{a}\frac{c}{a}\int_0^\infty \frac{ds}{\left(s+\frac{c^2}{a^2}\right)R(s)}, \tag{20}$$

where

$$R(s) = \sqrt{(s+1)\left(s+\frac{b^2}{a^2}\right)\left(s+\frac{c^2}{a^2}\right)}. \tag{21}$$

The demagnetizing factors along the other two directions have a similar form, with $[s+(c/a)^2]$ in the denominator of Eq. (20) replaced by $(s+1)$ or $[s+(b/a)^2]$, along the a axis or the b axis, respectively. We verify our numerical approach by calculating N for ellipsoids and find perfect agreement with Eq. (20).

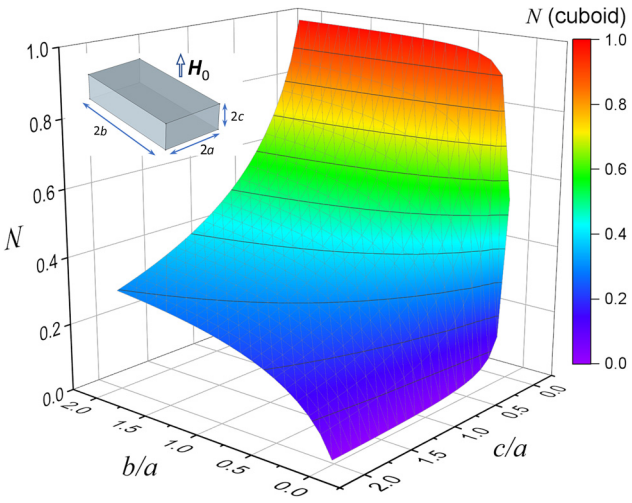

FIG. 4. The effective demagnetizing factor of a rectangular cuboid as a function of its two aspect ratios. The inset shows a schematic of the geometric arrangement.

B. The rectangular cuboid

The brick-shaped sample is most commonly encountered in research laboratories, because many single crystals tend to grow in this shape. The cutting and polishing procedure also favors this type of sample.

The three-dimensional surface of the effective demagnetizing factor, N, of a rectangular cuboid as a function of two aspect ratios, c/a and b/a, is shown in Fig. 4. Analysis of the numerical data leads us to suggest the simple formula

$$N_{\text{cuboid}} \approx \frac{4ab}{4ab+3c(a+b)}. \tag{22}$$

This is an important result of our work, because it describes the sample shape that is most frequently used. Note that Eq. (22) is an interpolation between the limiting cases of an infinitely thin sample ($c \to 0$, $N \to 1$) and $N \to 0$ in the opposite case.

The top panel of Fig. 5 shows the difference between the numerically calculated N for a rectangular cuboid (Fig. 4) and the approximation given by Eq. (22). For comparison,

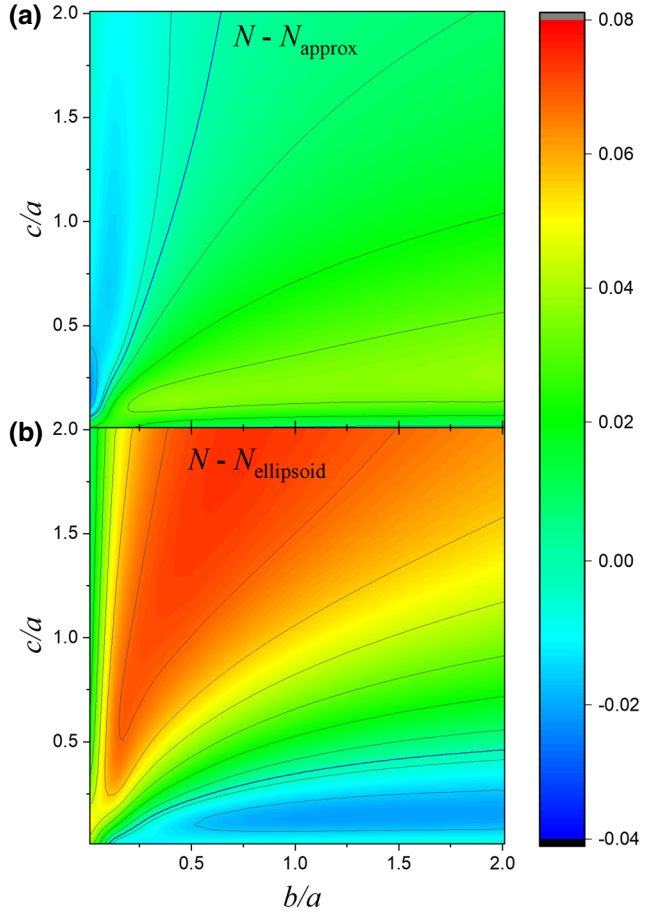

FIG. 5. (a) The the difference between the numerically calculated N and the approximation given by Eq. (22). (b) The difference between the numerically computed N for a cuboid and that for an ellipsoid, Eq. (20).

the bottom panel of Fig. 5 shows the difference between the numerically computed N for a cuboid and the analytic solution for an ellipsoid, given by Eq. (20). While the latter shows an upward deviation of 0.08 (considering that N can only vary between 0 and 1), the former remains a much closer function approximating the numerical results.

The relative error in determining the magnetic moment (and therefore the apparent susceptibility) of a finite sample due to a nonexact demagnetizing factor is readily derived from Eqs. (5) and (7):

$$\frac{m(N) - m(N_{\text{approx}})}{m(N)} = \frac{N_{\text{approx}} - N}{N_{\text{approx}} + \chi^{-1}}, \tag{23}$$

where N and N_{approx} are the exact and approximate demagnetizing factors, respectively, and χ is the intrinsic magnetic susceptibility. Estimates using Eq. (23) show that most of the diagram (except for very thin samples) in Fig. 5(a) results in errors within 10%. The error becomes larger for $b/a \gtrsim 1$ and $c/a \lesssim 0.1$ in the lower-right corner of Fig. 5(a). Indeed, if better precision is needed, full calculations are required.

By matching the magnetostatic self-energy to the total magnetic energy of a saturated ferromagnetic prism, Aharoni has provided formulas for the so-called "magnetometric" demagnetizing factor, N_m, of the rectangular prism [5]. Similarly, Pardo *et al.* has calculated both the "magnetometric" factor using the volume-average magnetic-field and "fluxmetric" factors using midplane average magnetic fields [6]. Both postulated that the sum of the three demagnetizing factors must be 1, which is not justified. However, when Pardo *et al.* relaxed this constraint in calculating their "magnetometric" N factors, their results agreed perfectly with our numerics for $c \le a$ [6]. Sato and Ishii provided very simple approximate formulas for square cuboids and circular cylinders of finite thickness in an axial magnetic field [7], which they obtained by analysis of the solutions of Aharoni and co-workers. They, therefore, agree well with Aharoni [5], but they disagree with our unconstrained numerical results. This is shown graphically in Fig. 6, where various effective demagnetizing N factors are shown for a square-base cuboid as a function of the thickness-to-side ratio, c/a.

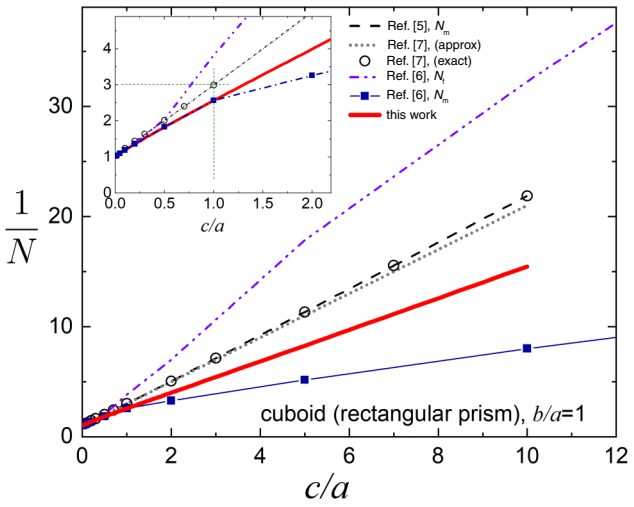

FIG. 6. A comparison of the effective demagnetizing factors for a square-base cuboid: this work (solid red line); "magnetometric," N_m, from Aharoni [5] (dashed black line); "magnetometric," N_m (solid squares), and "fluxmetric," N_f (dashed-double-dotted line), from Pardo *et al.* [6]; and magnetometric N factors—approximate (dotted grey) and exact (circles)—from Sato and Ishii [7]. The inset shows an enlargement at thinner samples. Of all the calculations, the magnetometric N factors calculated by Pardo *et al.* [6] are in very good agreement with our results for $c \le a$.

C. A finite cylinder in axial and transverse magnetic fields

1. A finite circular cylinder in an axial magnetic field

This is another typical shape of practical importance and interest. Often, it is a piece of a round wire, part of a superconducting magnet winding or various cables and transmission lines. It may be subject to either an axial or a transverse field (or a combination of the two). For the axial case (magnetic field along the cylinder axes) and a circular cross section, the inverse demagnetizing factor is

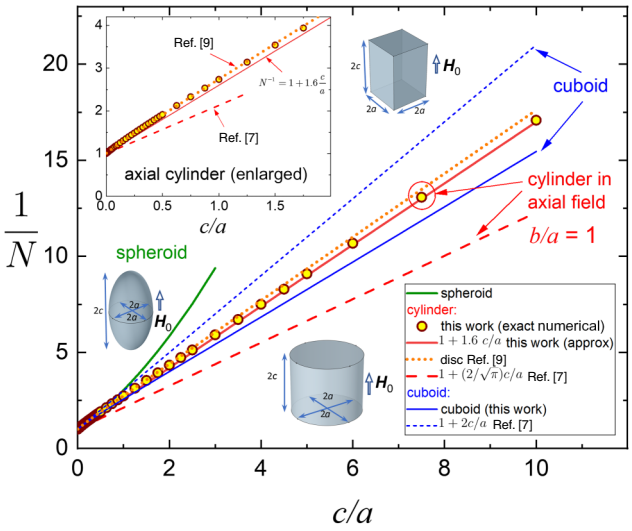

FIG. 7. The inverse of the effective demagnetizing factor, N^{-1}, as a function of the thickness-to-diameter aspect ratio for a cylinder. The open symbols are our numerical results and the solid line is our approximation, given by Eq. (24). For comparison, Brandt's theory is shown by the dotted line and the simplified approximations of Sato and Ishii by the dashed line. For completeness, comparative results for a cuboid are also shown by the solid line (this work) and the dashed line (from Ref. [7]). The inset shows an enlargement of the smaller-aspect-ratio region, showing excellent agreement between our numerical results and Brandt's formula [9].

shown in Fig. 7 and compared to a square-base cuboid and a spheroid of similar aspect ratio. For comparison, Fig. 7 also shows a rectangular cuboid and a spheroid as a function of the c/a ratio. Also shown is a comparison with formulas given by Sato and Ishii [7]. They approach our results in the thin limit, but the general trend is quite different.

As shown in Fig. 7, analysis of the numerical results shows that the simplest curves are obtained for the inverse of the effective demagnetizing factor N^{-1} as a function of the aspect ratio. Indeed, this has also been noted in many previous works; for example, Sato and Ishii [7] and Brandt [9]. In the case of a finite cylinder in an axial magnetic field, we obtain a simple approximate formula for the effective inverse demagnetizing factor:

$$N_{\text{axial}}^{-1} \approx 1 + 1.6\frac{c}{a}. \tag{24}$$

We note that our very early work suggested a similar approximation with a crude estimate of a numerical factor of 2 in place of 1.6 in Eq. (24) [10]. Our results can be compared with the numerical simulations of finite superconducting samples by Brandt [9]. He extended his calculations of infinite rectangular strips in a perpendicular magnetic field to finite disks of rectangular cross section. According to Brandt, for a disk of height $2c$ and diameter $2a$ [9],

$$N_{\text{disk}}^{-1} = 1 + \frac{1}{q}\frac{c}{a}, \tag{25}$$

where

$$q = \frac{4}{3\pi} + \frac{2}{3\pi}\tanh\left[1.27\frac{c}{a}\ln\left(1+\frac{a}{c}\right)\right]. \tag{26}$$

Figure 7 shows excellent agreement between our numerical results and Brandt's equations, lending further support to our calculations. On the other hand, the simplified approximations of Sato and Ishii [7] for these geometries do not agree at all with our results and those of Brandt.

2. A finite circular cylinder in a transverse magnetic field

We now consider a finite cylinder of circular cross section ($a = c$) in a magnetic field applied perpendicular to its axis. (Note that we change the designations of the dimensions compared to the previous subsection in order to follow the uniform naming scheme of this paper.) Figure 8 shows the inverse demagnetizing factor N^{-1} as a function of the a/b ratio. Note that this ratio is reciprocal to that of Eq. (24). For a small enough diameter-to-length ratio, a/b a good approximation for the demagnetizing factor in this case is the following:

$$N_{\text{transv}}^{-1} \approx 2 + \frac{1}{\sqrt{2}}\frac{a}{b}. \tag{27}$$

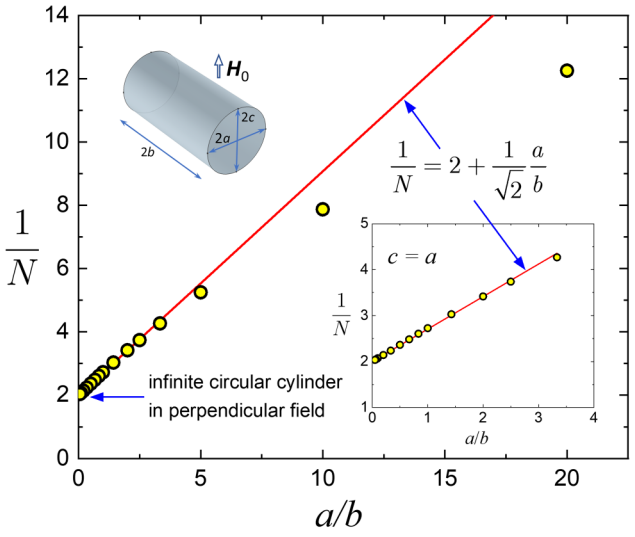

FIG. 8. A finite cylinder in a transverse magnetic field as a function of the ratio of the diameter to the length. The inset shows small a/b values.

Note that Eq. (27) gives the correct value of $N = 1/2$ for an infinite cylinder in a transverse field, $a/b \to 0$, and the correct value of $N = 0$ when $a/b \to$ inf.

3. Infinite rectangular and elliptical cross-section strips in a transverse field

Another significant case, which is a partial case of the general cuboid, is an infinite strip of rectangular cross section in a perpendicular field. This geometry is quite relevant for superconducting tapes as parts of cables or magnet windings. The demagnetizing correction here is an important ingredient of design optimization. It has been considered before by using a finite-element numerical approach similar to that used here, but in two dimensions [10] and also in a different way, using highly nonlinear $E(j)$ characteristics applicable for superconductors, by Brandt [9].

Figure 9 shows an inverse demagnetizing factor, N^{-1}, of an infinite strip of rectangular cross section as a function of the thickness-to-width ratio, c/a. The inset shows a smaller range of c/a values. Two simple approximate formulas are as follows:

$$N_{\text{inf-rect-strip}}^{-1} = \begin{cases} 1 + \frac{2}{3}\frac{c}{a}, & \text{large } \frac{c}{a} \gtrsim 5, \\ 1 + \frac{3}{4}\frac{c}{a}, & \text{small } \frac{c}{a} \lesssim 5. \end{cases} \tag{28}$$

Using numerical simulations of finite superconducting samples, Brandt [9] gives

$$N_{\text{inf-rect-strip}}^{-1} = 1 + \frac{1}{q}\frac{c}{a}, \tag{29}$$

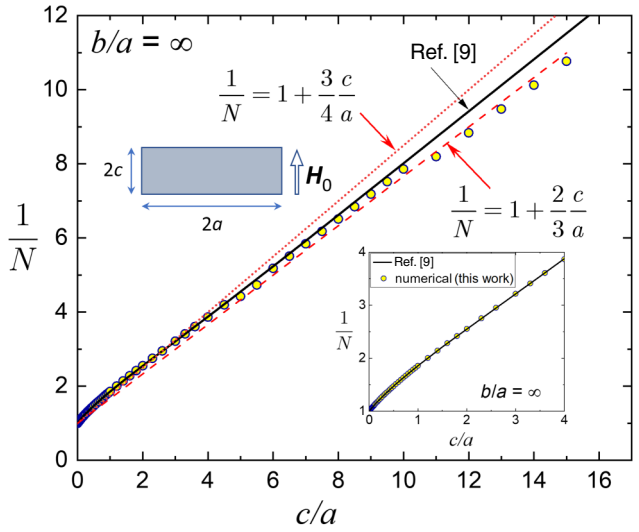

FIG. 9. The inverse demagnetizing factor, N^{-1}, of an infinite strip of rectangular cross section as a function of the thickness-to-width ratio, c/a. Two simple approximate formulas are shown. Also shown is the more elaborate formula by Brandt [9], which agrees quite well with the numerical results up to $c/a = 10$. The inset shows a smaller range of c/a values.

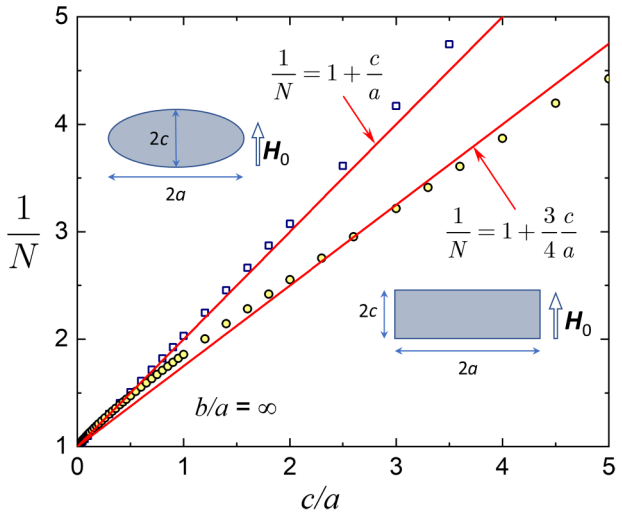

FIG. 10. The inverse demagnetizing factor of an infinite strip of elliptical cross section compared to a strip of rectangular cross section. Both are infinite in the b direction.

where

$$q = \frac{\pi}{4} + 0.64 \tanh\left[0.64\frac{c}{a}\ln\left(1.7 + 1.2\frac{a}{c}\right)\right]. \qquad (30)$$

Notably, for a square cross-section ($a = c$) strip that is infinite along the b direction, Brand obtained $N_a = N_c = 0.538$, also noting that the sum of the demagnetizing factors is greater than 1 for nonellipsoidal shapes (the third factor, $N_b = 0$ for an infinite strip).

Next, Fig. 10, we consider an infinite strip of elliptical cross section, compared to a rectangular strip. It turns out that the elliptical cross section has the simplest approximate equation for the effective demagnetizing factor of all the considered cases. Here,

$$N^{-1}_{\text{inf-ell-strip}} \approx 1 + \frac{c}{a}. \qquad (31)$$

D. Exotic geometries

The described numerical method allows for the calculation of the effective demagnetizing correction for samples of any shape. For an illustration, let us consider a pyramid in the shape of the Great Pyramid of Giza, a cone inscribed in this pyramid, and a slab enclosing it, all three being shown in Fig. 11. In all these cases, the ratio of the height to the side is $c/a = 2/\pi \approx 0.64$. It is most likely a pure coincidence, but the demagnetizing factor of the Great Pyramid (and of the inscribed cone), $N = 0.64$, is the same as the ratio of the height to the side. For a cuboid of the same c and a, the value $N = 0.49$ is smaller owing to the larger volume compared to the cross-sectional area responsible for the magnetic-field distortion around the sample. This adds yet another puzzle for Egyptologists.

VII. CONCLUSIONS

We introduce a direct assumptions-free efficient way to estimate the effective (or "integral") demagnetizing factors of arbitrarily shaped diamagnetic samples. The key equation, Eq. (9), is generalized and rederived in the form of Eq. (8) where vector $\mathcal{E}(\boldsymbol{\rho}) = \int d^3\boldsymbol{r}\boldsymbol{R}/R^3$ can be interpreted as a pseudoelectric field $\mathcal{E}$ produced by a charge

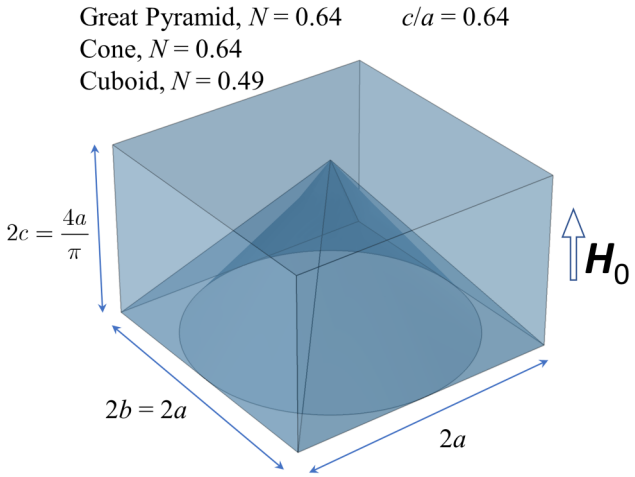

FIG. 11. "Exotic" sample shapes: the Great Pyramid of Giza, an inscribed cone of the same height, and a cuboid enclosing the pyramid. The effective demagnetizing factor of the pyramid (and the same for the inscribed cone), $N = 0.64$, is the same as the ratio of the height to the side, $c/a = 2/\pi = 0.64$. For a cuboid with the same height and side, $N = 0.49$.

TABLE I. The approximate effective ("integral") demagnetizing factor along an applied magnetic field.

Shape	Geometry	Demagnetizing factor along applied field
Ellipsoid (exact)	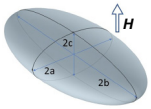	$N=\frac{1}{2}\frac{b}{a}\frac{c}{a}\int_0^\infty \frac{ds}{\left(s+\frac{c^2}{a^2}\right)\sqrt{(s+1)\left(s+\frac{b^2}{a^2}\right)\left(s+\frac{c^2}{a^2}\right)}}$
Rectangular cuboid	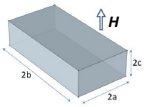	$N^{-1}=1+\frac{3}{4}\frac{c}{a}\left(1+\frac{a}{b}\right)$
Strip, rectangular		$N^{-1}=1+\frac{2}{3}\frac{c}{a}$ for $(c/a\gtrsim 5)$, $=1+\frac{3}{4}\frac{c}{a}$ for $(c/a\lesssim 5)$
Strip, elliptical	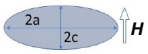	$N^{-1}=1+\frac{c}{a}$
Cylinder, axial	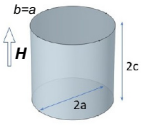	$N^{-1}=1+1.6\frac{c}{a}$
Cylinder, transverse	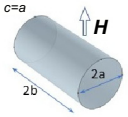	$N^{-1}=2+\frac{1}{\sqrt{2}}\frac{a}{b}$
Great pyramid (cone, cuboid)	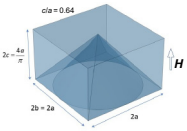	$N=0.64$ $(0.64, 0.49)$

density -1 uniformly distributed in the entire space, and the particular form of $\mathcal{E}(\boldsymbol{r})$ depends on the shape of the integration domain. This answers the question posed in Sec. I. Namely, it allows the calculation of the total magnetic moment of an arbitrarily shaped sample if the volume distribution of the magnetic induction is known. In this work, the latter is obtained from adaptive finite-element full 3D numerical calculations using the COMSOL 5.3 software. We provide simple approximate, yet accurate [e.g., for a cuboid within $\Delta N<0.05$, see Fig. 5(a)], analytic expressions to estimate the effective demagnetizing factors of samples of commonly used nonellipsoidal shapes, which are summarized in Table I.

ACKNOWLEDGMENTS

This work was supported by the U.S. Department of Energy (DOE), Office of Science, Basic Energy Sciences, Materials Science and Engineering Division. Ames Laboratory is operated for the U.S. DOE by Iowa State University under Contract No. DE-AC02-07CH11358.

APPENDIX A: THE CURRENT RING

To demonstrate how calculations of the total magnetic moment work, it is instructive to consider an example of a ring of a radius $a=1$ m in plane $z=0$ with current $J/4\pi=1$ A. The total magnetic moment is $m_z=J\pi a^2=4\pi^2$ Am^2. The field B_z around the ring according to Landau is [1]

$$B_z=\frac{2}{\sqrt{(1+r)^2+z^2}}\left[\boldsymbol{K}+\frac{1-r^2-z^2}{(1-r)^2+z^2}\boldsymbol{E}\right], \tag{A1}$$

where r,z are cylindrical coordinates, and the complete elliptic integrals $\boldsymbol{K},\boldsymbol{E}$ are functions of $k^2=4r/[(1+r)^2+z^2]$. The Jackson theorem for this case with no applied field reads as follows:

$$\frac{2}{3}m=\int B_z dV, \tag{A2}$$

where the integration is over the whole space. Hence, one has to check the equality

$$\int B_z d^3\boldsymbol{r} = \frac{8\pi^2}{3}. \tag{A3}$$

One can perform the volume integration in spherical coordinates R,θ: $r = R\sin\theta$, $z = R\cos\theta$, and $dV = 2\pi R^2 \sin\theta dR\, d\theta$:

$$B_z = \frac{2}{\sqrt{1+2R\sin\theta+R^2}}\left[\boldsymbol{K} + \frac{1-R^2}{1-2R\sin\theta+R^2}\boldsymbol{E}\right],$$
$$k^2 = \frac{4R\sin\theta}{1+2R\sin\theta+R^2}. \tag{A4}$$

The integral is readily calculated numerically: $\int B_z d^3\boldsymbol{r} \approx 26.32$ coincides with the analytic value $8\pi^2/3$ and gives $m = 3I_z/2 = 4\pi^2 \approx 39.48$.

Another way of evaluating the integral $\boldsymbol{I}$ in the whole space is to choose cylindrical integration elements with their axis along the applied field $\mathbf{H_0} = H_0\hat{z}$. To this end, we use Eq. (A1), where B_z is given in cylindrical coordinates. The numerical integration yields $I_z = 39.48$, which coincides with the result for spherical integration multiplied by 3/2. Equation (B8) gives $m_z = I_z = 4\pi^2 \approx 39.48$. Thus, although the results of numerical evaluation of the integral over the whole space differ from those of the spherical method, the magnetic moment value for the two methods turns out to be the same.

To illustrate how our numerical calculations reproduce the nontrivial analytic results presented here, Fig. 12 shows an evaluation of the z component of the integral I, given in Eq. (B1), using spherical and cylindrical shells. The inset in Fig. 12 shows a three-dimensional pie-cut picture of the absolute value of the magnetic induction around the ring. The ring radius, $= 1/\sqrt{\pi}$ m, is chosen to have a ring area that gives a total magnetic moment of 1 Am^2 with 1 A current in the ring. With such a choice, the value of the integral $\boldsymbol{I}$ will be equal to $1/\alpha$ of Eq. (9). Note that the numerical calculations here and everywhere in this paper are carried out in SI units. We obtain that the spherical-shell integration tends to the value of $\alpha^{-1} = 2/3$ and the cylindrical-shell integration to $\alpha^{-1} = 1$, exactly as shown analytically. Moreover, both integrals stop changing as soon as the sample current is fully enclosed in the integration volume, again as expected from the analytic calculations. Therefore, integration of space outside the sample does not contribute to the integral $\boldsymbol{I}$. This does not mean, however, that the outer space can be truncated for numerical calculations. It should still be much larger compared to the sample size in order to solve for a (very-long-range) magnetic-field distribution correctly.

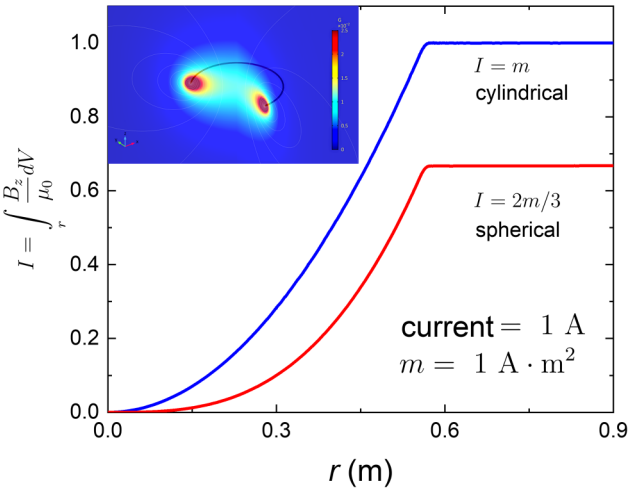

FIG. 12. Integral I_z, of Eq. (B1), calculated numerically using spherical shells and cylindrical shells, respectively. The calculations are done in SI units and the ring radius [$= 1/\sqrt{(\pi)}$ m] is chosen to give a total magnetic moment of 1 Am^2 for a current of 1 A. In this way, the integral value is just $1/\alpha$ of Eq. (9). The inset shows a three-dimensional pie-cut picture of the absolute value of the magnetic induction around the ring.

APPENDIX B: THE EQUATION (9) IN GAUSSIAN UNITS

The derivation of this identity is given in the main text in the "recommended" SI system, which is also used in COMSOL, to solve the Maxwell equations for the field distribution in SI units. This, however, makes the derivation unnecessarily cumbersome. Many researchers working in the fields of superconductivity and magnetism prefer CGS and it is also used in magnetometers such as Quantum Design's Magnetic Property Measurement System (MPMS). Therefore, here we provide the same derivation in the Gaussian system, which, in our opinion, makes the derivation more transparent.

The total magnetic moment $\boldsymbol{m}$ of a finite-size sample is proportional to the volume integral of the total field distribution $\boldsymbol{B}(\boldsymbol{r})$ over a sphere of large enough radius $\mathcal{R}_1$ such that the whole sample is situated inside the sphere. This statement is proven in Jackson [12], which gives the following:

$$\boldsymbol{I} = \int_{r<\mathcal{R}} [\boldsymbol{B}(\boldsymbol{r}) - \boldsymbol{H}_0] d^3\boldsymbol{r} = \frac{8\pi}{3}\boldsymbol{m}. \tag{B1}$$

Here, $\boldsymbol{H}_0$ is the applied field. In particular, one can take $\mathcal{R} \to \infty$, i.e., the integral can cover the whole space. This identity is proven in Ref. [12] by expanding the field outside a sphere $\mathcal{R}$ that contains the sample (the currents) in spherical harmonics. From the point of view of a finite-element numerical method, it is more convenient

to deal with cylindrical integration domains. We thus provide a proof that is not related to a particular shape of the integration region.

The field $\boldsymbol{B}$ consists of the applied field and the field $\boldsymbol{b}$ due to currents $\boldsymbol{J}$ in the sample of a finite volume V:

$$\boldsymbol{B} = \boldsymbol{H}_0 + \boldsymbol{b}, \tag{B2}$$

i.e., $\boldsymbol{I} = \int \boldsymbol{b} d^3\boldsymbol{r}$, where, according to the Biot-Savart law,

$$\boldsymbol{b}(\boldsymbol{r}) = \frac{1}{c}\int_V d^3\boldsymbol{\rho}\frac{\boldsymbol{J}(\boldsymbol{\rho})\times\boldsymbol{R}}{R^3}, \quad \boldsymbol{R} = \boldsymbol{r} - \boldsymbol{\rho}. \tag{B3}$$

Hence, we have

$$\begin{aligned} c\boldsymbol{I} &= \int d^3\boldsymbol{r}\int_V d^3\boldsymbol{\rho}\frac{\boldsymbol{J}(\boldsymbol{\rho})\times\boldsymbol{R}}{R^3} \\ &= \int_V d^3\boldsymbol{\rho}\,\boldsymbol{J}(\boldsymbol{\rho})\times\int d^3\boldsymbol{r}\frac{\boldsymbol{R}}{R^3}, \end{aligned} \tag{B4}$$

where the integration over $\boldsymbol{r}$ is extended to the whole space.

The vector $\mathcal{E}(\boldsymbol{\rho}) = \int d^3\boldsymbol{r}\boldsymbol{R}/R^3$ is analogous to the electrostatic field of a charge distribution with density of -1 in the whole space. For such a distribution, the field $\mathcal{E}$ is not defined uniquely, it depends on the way in which one divides the space into charged elements.

For $\boldsymbol{\rho} = 0$, we must have $\mathcal{E} = \int \mathbf{d^3}\boldsymbol{r}(\boldsymbol{r}/\mathbf{r^3}) = \mathbf{0}$ by symmetry. If one uses elements as spherical shells, and applies the Gauss theorem to a sphere of a radius ρ, one obtains:

$$\mathcal{E} = -\frac{4\pi}{3}\boldsymbol{\rho}. \tag{B5}$$

Hence, we have

$$\boldsymbol{I} = -\frac{4\pi}{3c}\int_V d^3\boldsymbol{\rho}\,\boldsymbol{J}(\boldsymbol{\rho})\times\boldsymbol{\rho} = \frac{8\pi}{3}\boldsymbol{m}, \tag{B6}$$

where $\boldsymbol{m}$ is the total magnetic moment. It is worth noting that this formula holds for any current distribution within the finite sample of arbitrary shape.

If one uses elements as cylindrical shells parallel to $\boldsymbol{H}_0$, i.e., one chooses the volume element as $2\pi\rho_1\, d\rho_1 dz$ (in which $\boldsymbol{\rho}_1$ is the cylindrical radius vector), and applies the Gauss theorem to a cylinder of a radius ρ, one obtains:

$$\mathcal{E} = -2\pi\boldsymbol{\rho}_1. \tag{B7}$$

where $\boldsymbol{\rho}_1$ is now the cylindrical radius vector. Substituting this in Eq. (B4), one expresses the z component of the integral $\boldsymbol{I}$:

$$I_z = 4\pi m_z. \tag{B8}$$

[1] L. D. Landau and E. M. Lifshitz, in *Electrodynamics of Continuous Media*, edited by E. M. Lifshitz, L. P. Pitaevskii (translated by J. B. Sykes, J. S. Bell, and M. J Kearsley) (Pergamon Press, 1984), 2nd ed., Vol. 8.

[2] J. A. Osborn, Demagnetizing factors of the general ellipsoid, Phys. Rev. **67**, 351 (1945).

[3] R. I. Joseph and E. Schlmann, Demagnetizing field in nonellipsoidal bodies, J. App. Phys. **36**, 1579 (1965).

[4] D. X. Chen, J. A. Brug, and R. B. Goldfarb, Demagnetizing factors for cylinders, IEEE Trans. Mag. **27**, 3601 (1991).

[5] A. Aharoni, Demagnetizing factors for rectangular ferromagnetic prisms, J. App. Phys. **83**, 3432 (1998).

[6] E. Pardo, D.-X. Chen, and A. Sanchez, Demagnetizing factors for completely shielded rectangular prisms, J. App. Phys. **96**, 5365 (2004).

[7] M. Sato and Y. Ishii, Simple and approximate expressions of demagnetizing factors of uniformly magnetized rectangular rod and cylinder, J. App. Phys. **66**, 983 (1989).

[8] A. Smith, K. K. Nielsen, D. V. Christensen, C. R. H. Bahl, R. Bjrk, and J. Hattel, The demagnetizing field of a nonuniform rectangular prism, J. App. Phys. **107**, 103910 (2010).

[9] E. H. Brandt, Geometric edge barrier in the Shubnikov phase of type-II superconductors, Low Temp. Phys. **27**, 723 (2001).

[10] R. Prozorov, R. W. Giannetta, A. Carrington, and F. M. Araujo-Moreira, Meissner-London state in superconductors of rectangular cross section in a perpendicular magnetic field, Phys. Rev. B **62**, 115 (2000).

[11] COMSOL version 5.3, Multiphysics reference manual, and AC/DC module user's guide, www.comsol.com, COMSOL Inc. (2017).

[12] J. D. Jackson, *Classical Electrodynamics* (John Wiley & Sons, New York, 1999), 3rd ed.

[13] P. M. Morse and H. Feshbach, *Methods of Theoretical Physics* (McGraw-Hill, New York, 1953), part II, Section 10.3.

[14] W. T. Doyle and I. S. Jacobs, The influence of particle shape on dielectric enhancement in metal-insulator composites, J. App. Phys. **71**, 3926 (1992).